Pergamon

*Int. J. Mech. Sci.* Vol. 36, No. 10, pp. 897–910, 1994

0020-7403/94 $7.00 + 0.00

0020-7403(94)E0032-E

# THE INFLUENCE OF STRAIN-PATH CHANGES ON FORMING LIMIT DIAGRAMS OF Al 6111 T4

ALEJANDRO GRAF and WILLIAM HOSFORD
Department of Materials Science and Engineering, The University of Michigan, Ann Arbor, MI 48109, U.S.A.

(*Received* 28 *June* 1993; *and in revised form* 3 *December* 1993)

**Abstract**—The effects of changing strain-paths on forming limits of aluminum alloy 6111 T4 have been investigated by determining forming limit diagrams (FLDs) of specimens prestrained to several levels in uniaxial, plane strain and biaxial tension, parallel and perpendicular to the prior rolling direction. Prestraining in biaxial tension generally lowers the entire FLD, whereas prestraining in uniaxial tension raises the limits on the right hand side of the FLD without much effect on the left hand side, when the direction of the largest principal strain does not change. If the directions of the principal strains are rotated, prestraining in uniaxial or plane strain tension lowers the forming limits for most of the FLD range.

A general finding was that, after prestraining, the amount of the additional plane strain deformation possible before failure depends on the effective strain during prestrain, regardless of the original strain-path. Finally, an example of the importance of strain-path changes in a stamping of an aluminum automobile part is presented.

## NOTATION

| | |
|---|---|
| $\varepsilon_1$, $\varepsilon_2$ | major and minor principal strains in the plane of the sheet |
| $\varepsilon_3$ | thickness strain |
| $\bar{\varepsilon}$ | effective strain |
| $\rho$ | strain ratio $\varepsilon_2/\varepsilon_1$ |
| $R_0$, $R_{45}$, $R_{90}$ | ratios of minor to through thickness strains in uniaxial tension at 0, 45 and 90° to the rolling direction |
| $\bar{R}$ | average strain ratio |
| $\Delta R$ | planar anisotropy parameter |
| $\sigma_1$, $\sigma_2$ | major and minor principal stresses in the plane of the sheet |
| $\bar{\sigma}$ | effective stress |
| $\alpha$ | stress ratio $\sigma_2/\sigma_1$, with $\sigma_3 = 0$ |
| $\zeta$ | ratio of major to effective stresses, $\sigma_1/\bar{\sigma}$ |
| $k$ | pre-exponent in the power-law hardening equation |
| $n$ | exponent in the power-law hardening equation |
| $m$ | strain-rate sensitivity coefficient |
| $\sigma_y$ | yield strength |
| $\sigma_u$ | tensile strength |
| $\varepsilon_{2f}$, $\varepsilon_{3f}$ | fracture strains in the minor and thickness directions |
| $dw$ | plastic work increment |
| $d\varepsilon_1$, $d\bar{\varepsilon}$ | strain increments |
| $\theta$ | angle measured from rolling direction |

## INTRODUCTION

Very often, stamped sheet parts undergo strain-path changes during stamping operations. These may be gradual, as metal flows through the die, or abrupt, when metal is transferred from one press to another. The influence of strain-path changes on formability is known by stamping engineers, who occasionally note that, in regions without evidence of localized necking, the strains are well above the accepted limits, as expressed by the forming limit diagram (FLD) [1], and that sometimes necking failures occur in regions where the strains are well below the forming limits. There have been a number of papers on the influence of strain paths on FLDs for low carbon steel sheets [2–5] but very little work has been done for aluminum sheets [6].

The ways that the strain limits change with prestrain vary with materials [7], making generalization difficult, even for alloys of the same base material [6]. Thus, it is important to document the FLDs of aluminum alloys, particularly because their formability is generally poorer than that of low-carbon steel. A recent paper by the authors [8] dealt with the effects of abrupt strain-path changes on the FLDs of aluminum alloy 2008 T4. This paper deals with experiments on aluminum alloy 6111 T4.

## EXPERIMENTAL

The sheets were 1.05 mm thick, with an approximate chemical composition of 0.85% Si, 0.75% Cu, 0.65% Mg, 0.25% Fe, 0.22% Mn, 0.03% Cr and 0.03% Zn, with the balance being aluminum. The microstructure consisted of pancake-shaped grains. The average intercept length of random lines on the cross section was 22 $\mu$m and the average intercepts in the principal directions were about 17 $\mu$m normal to the sheet and 40 $\mu$m parallel to both the rolling and transverse directions.

The results of duplicate tension tests at 0, 45 and 90° are given in Table 1. The strain ratio $R = \varepsilon_2/\varepsilon_3$, the yield strength $\sigma_y$ and $k$ and $n$ in the Hollomon equation $\bar{\sigma} = k\bar{\varepsilon}^n$ were determined on tests using specimens with parallel sides. The slightly lower value of $n$ in the rolling direction is consistent with the lower elongation. The decrease of $n = \mathrm{d}(\ln\sigma)/\mathrm{d}(\ln\varepsilon)$ with strain is similar to the behavior of Al 2008–T4 and suggests that the power-law hardening equation does not describe the stress–strain relation completely, although the correlation coefficients for the fit are greater than 0.999. Nevertheless, it is used widely for metallic sheets. The $R$ values reported were obtained by measuring the length and width strains after 15% elongation. Similar strain ratios were obtained after 5 and 10% elongation, suggesting the strain independence of this parameter. The average strain ratio is $\bar{R} = (R_0 + R_{90} + 2R_{45})/4 = 0.68$ and $\Delta R = (R_0 + R_{90} - 2R_{45})/2 = 0.09$. The tensile strength, $\sigma_u$, percent elongation and stain-rate exponent, $m$, were found from tests using standard tensile specimens.

The fact that the percent elongation converted to true strain is less than the value of $n$ can be attributed to the gradual decrease of $n$ with strain. The negative rate sensitivity and taper of standard specimens may also have contributed to this finding. The strain-rate sensitivity was calculated from changes in the force, $F$, accompanying abrupt changes in crosshead speed, $V$, for six different jump tests. In each case $-0.004 \leqslant m \leqslant -0.003$. The experimental techniques for prestraining, measuring strains and determining FLDs are detailed elsewhere [8].

## RESULTS

Figure 1 combines two FLDs for the as-received material, one with the larger principal strain, $\varepsilon_1$, parallel to the transverse direction (TD), and the other with $\varepsilon_1$ parallel to the

TABLE 1. SUMMARY OF TENSILE TESTS RESULTS

| Orientation/number | 0° | | 45° | | 90° | |
|---|---|---|---|---|---|---|
| Test number | 1 | 2 | 1 | 2 | 1 | 2 |
| $n$ ($0.05 \leqslant \varepsilon \leqslant 0.20$) | 0.252 | 0.257 | 0.261 | 0.259 | 0.256 | 0.257 |
| $k$(MPa) | 561 | 564 | 557 | 555 | 554 | 554 |
| $n$ ($0.10 \leqslant \varepsilon \leqslant 0.20$) | 0.239 | 0.242 | 0.251 | 0.249 | 0.244 | 0.246 |
| $k$(MPa) | 548 | 549 | 547 | 545 | 540 | 543 |
| $\sigma_y$(MPa) | 184 | 185 | 170 | 168 | 165 | 165 |
| $\sigma_u$(MPa) | 305 | 305 | 299 | 299 | 299 | 299 |
| Elongation(%) | 25.6 | 25.9 | 27.8 | 28.0 | 27.8 | 29.6 |
| $R$† | 0.68 | 0.65 | 0.62 | 0.64 | 0.80 | 0.77 |

†Obtained after 15% strain. Additional $R$ values were determined: $R_{22.5°} = 0.75$ and $R_{67.5°} = 0.59$.

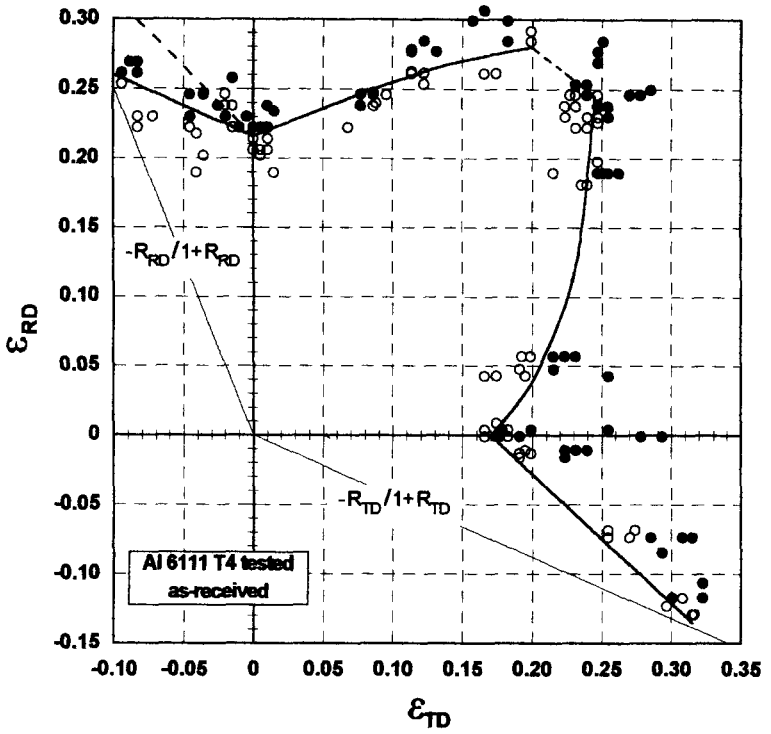


FIG. 1. FLD of as-received material. The lines labeled $-R/1+R$ are the strain-paths in tension tests. The upper left dashed line corresponds to a constant thinning ($\varepsilon_3$) criterion for failure.

rolling direction (RD). The fact that the forming limit in plane strain with $\varepsilon_1$ parallel to TD is lower than in plane strain with $\varepsilon_1$ parallel to RD can be attributed to the ridging tendency of the sheet. When the sheet is strained with $\varepsilon_1$ parallel to the TD (or in biaxial tension), it develops a topology of hills and valleys parallel to the rolling direction. The valleys tend to localize the deformation, lowering the forming limits. Takakura *et al.* [9] showed that eliminating roughness raises the forming limits for aluminum and copper.

The ridging also affects the failures in near equibiaxial tension. In these tests, the necks always formed parallel to RD, which is characteristic of tests with $\varepsilon_1$ parallel to TD. The change in neck orientation causes a discontinuity in the combined FLD, indicated by the dashed portion near to equibiaxial tension. Data on the right hand side, between plane strain and equibiaxial stretching, could not be generated with the conventional specimens because they failed prematurely near the binder. To overcome this, a much larger binder diameter (250 mm vs usual 140 mm) was used with specimen widths of 208, 218 and 222 mm. A deformed specimen is shown in Fig. 2.

Although the forming limits left of plane strain usually follow a line of constant thinning strain ($\varepsilon_3$), this is not true for the FLD with $\varepsilon_1$ parallel to the RD, where there is less thinning in uniaxial tension than in plane strain.

Table 2 shows the thickness strains, $\varepsilon_{3f}$, at fracture for several loading paths. Also shown are the corresponding values of $\varepsilon_{2f}$ which equal $\varepsilon_2$ outside the neck. The values of $\varepsilon_{1f}$ could not be measured because of the sharpness of the necks. Note that specimens tested with $\varepsilon_1$ parallel to RD reached higher strains than those tested with $\varepsilon_1$ parallel to TD.

*FLDs of sheets prestrained in equibiaxial tension*

Figure 3 gives the FLDs for sheets prestrained in equibiaxial tension. The individual data for one prestrain are shown in Fig. 3(a) and (b) summarizes the curves for various levels of prestrain. In each case, $\varepsilon_1$ after the prestrain was normal to the RD. Duplicate specimens were used to locate the positions of the minima. In general, prestraining shifted the minima to the right, lowering the forming limits in most of the region right of plane strain.

For equibiaxial tension, prestraining raised the failure limit. This is surprising, because in this case there was no strain-path change (both pre- and final straining were in equibiaxial tension). The only difference between these tests and the continuous tests on as-received material was a period of time between the initial and final stretching, which suggests that

TABLE 2. FRACTURE STRAINS FOR SEVERAL LOADING PATHS

| Strain state | Uniaxial tension ∥RD | Uniaxial tension ⊥RD | Plane strain tension ∥RD | Plane strain tension ⊥RD | Biaxial tension |
|---|---|---|---|---|---|
| $\varepsilon_{2f}$ | − 0.10 | − 0.13 | 0 | 0 | 0.25 |
| $\varepsilon_{3f}$ | − 0.82 | − 0.64 | − 0.71 | − 0.51 | − 0.65 |

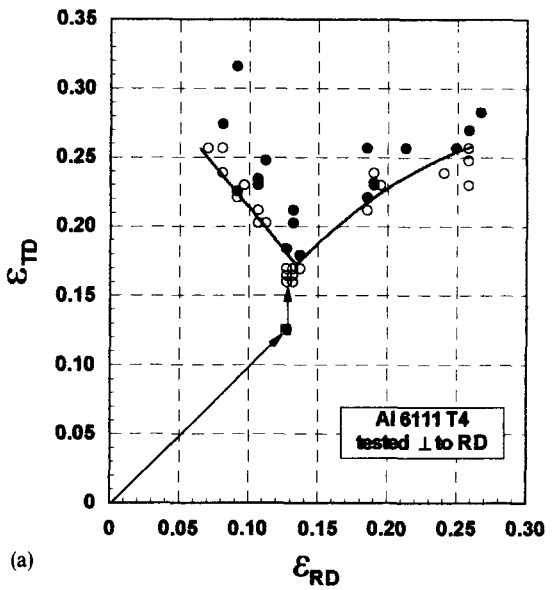


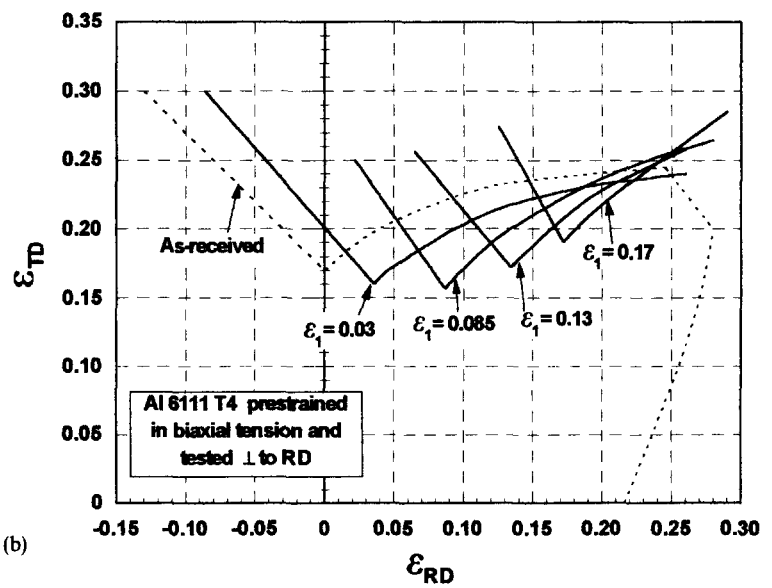


FIG. 3. (a) FLD after biaxial prestraining $\varepsilon = 0.13$; and (b) FLDs for as-received and equibiaxially prestrained sheets. Note that prestraining increases the strain limits in biaxial tension.


FIG. 2. FLD specimen used to obtain intermediate strain states between plane strain and equibiaxial tension. The binder diameter is 250 mm.

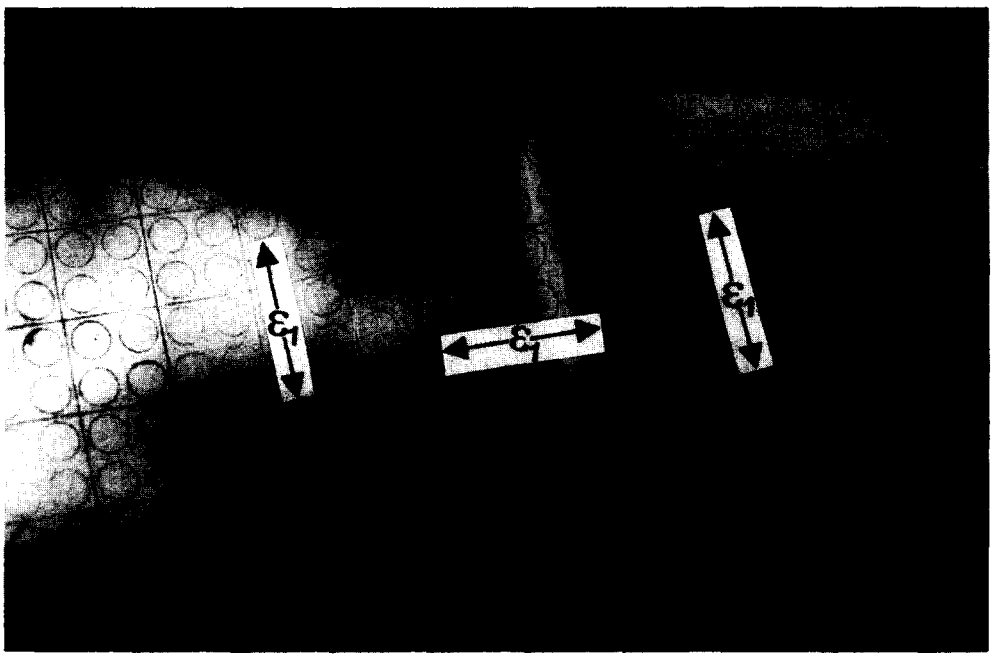


(a)

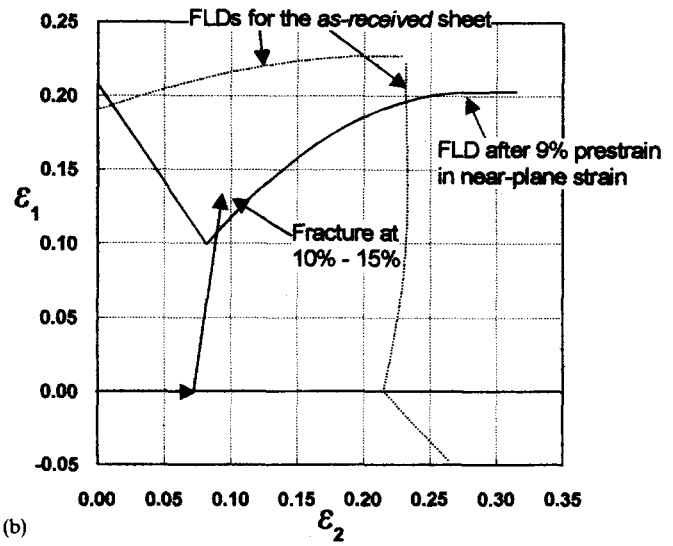


(b)

FIG. 10. (a) Partial view of a car door frame. The major strains directions at different locations are indicated by the arrows. The minor strain at the split site is very close to the major strain prevailing at both sides of it. This indicates that additional plane strain 90° to the original one was imposed at the end of the punch travel; and (b) the strain state at the split site in (a) below the FLD for the as-received, material but the failure can be explained by considering how the FLD was altered by the change in strain-path.

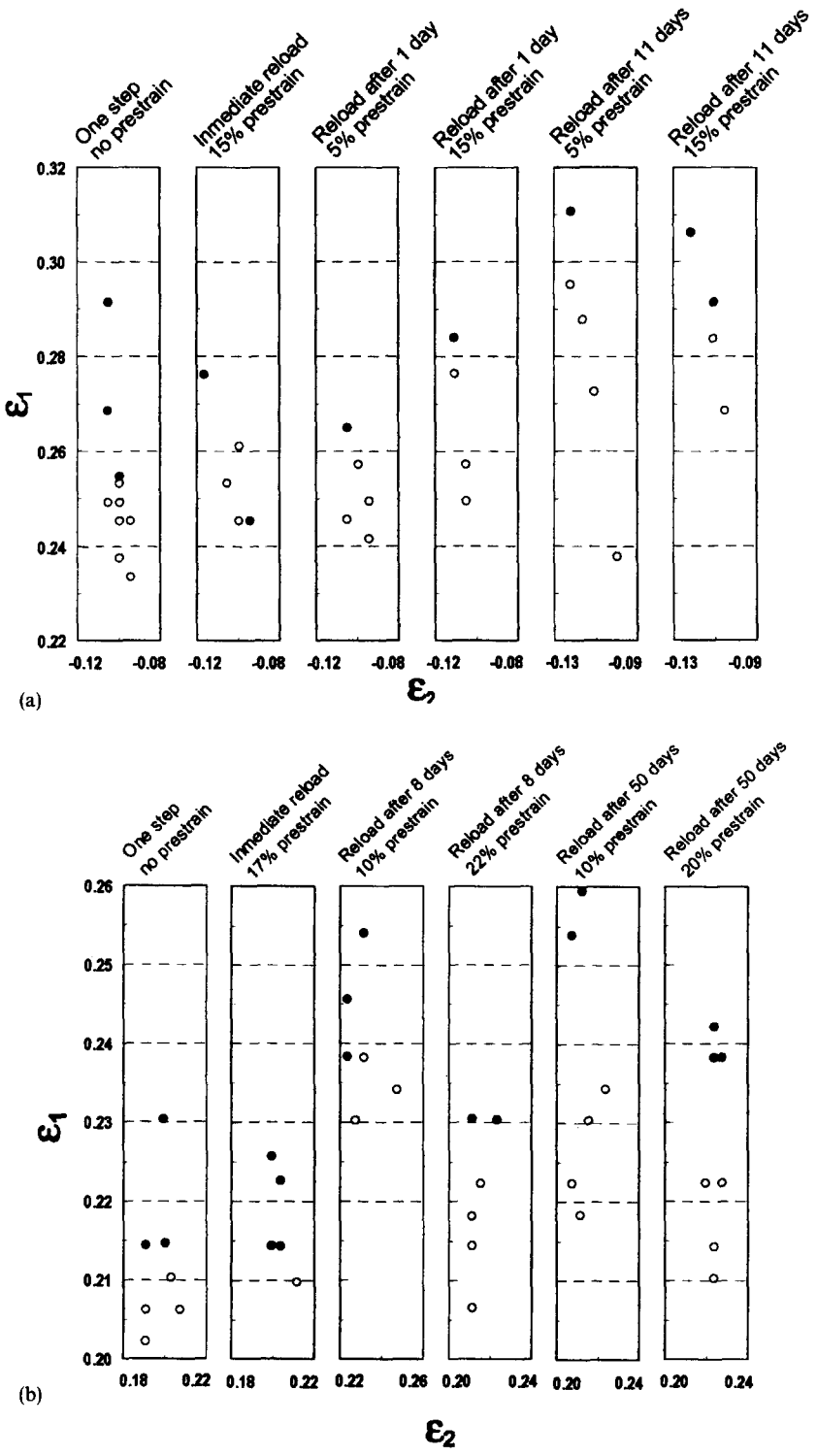


FIG. 4. (a) Strain limits in uniaxial tension parallel to the RD after interrupting the tests at two levels of uniaxial prestrain and waiting different periods of time before reloading; and (b) strain limits in equibiaxial tension after imposing two levels of equibiaxial prestrains and waiting different periods of time before reloading.

some recovery may have occurred during this interval and that this recovery increased the failure strain. To check this hypothesis, tests were run in uniaxial and in biaxial tension, in which the straining was interrupted for various periods of time after several levels of prestrain. The results in Fig. 4 show that interruptions of a day or more raised the failure

strains by 2–5% over those obtained in continuous or with immediate reloading tests. Additional delay beyond a few days had little effect.

*FLDs of sheets prestrained in uniaxial tension*

Two different strain path combinations were used: (1) both prestrain and final testing with $\varepsilon_1$ normal to RD; and (2) prestrain with $\varepsilon_1$ parallel to RD and final testing with $\varepsilon_1$ normal to RD. In the latter case, the rotation of the principal strains' directions produces a large degree of strain reversal.

Figure 5 shows the FLDs for case (1). The data for an individual FLD are shown in Fig. 5(a) and (b) summarizes the FLDs after different uniaxial prestrains. For a low prestrain

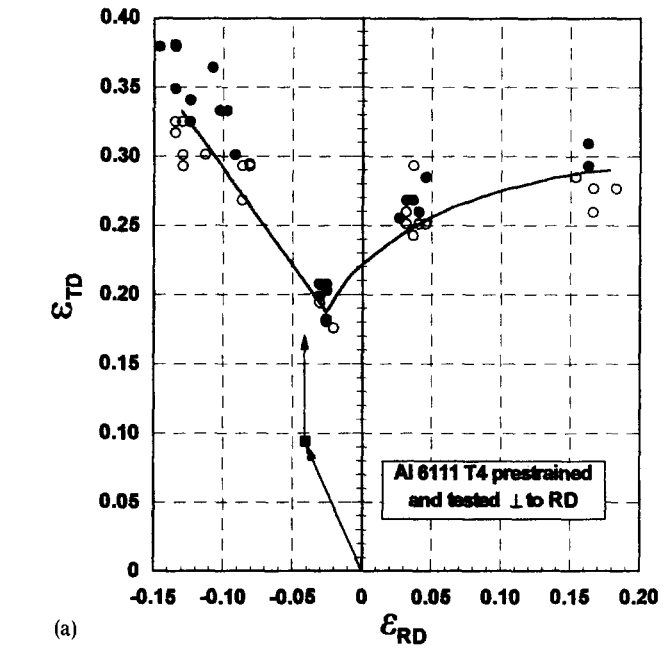


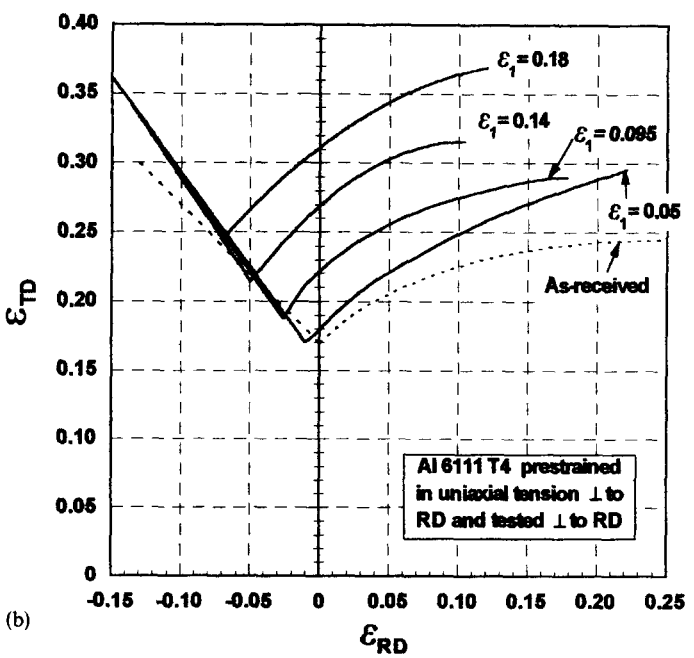


FIG. 5. (a) FLD after uniaxial prestrain $\varepsilon_1 = 0.095$ normal to RD; and (b) FLDs obtained for $\varepsilon_1$ normal to the RD after prestraining in uniaxial tension normal to the RD. Note the constant thinning trend for the left hand side that does not project to FLDo.

( $\approx$ 5%) the FLD is shifted only to the left and then with increasing prestrain, the FLDs are shifted upward and to the left approximately along a line of constant thinning. In each of these FLDs, in the subsequent loading after prestraining in uniaxial tension, the minimum occurs slightly ($\Delta\varepsilon \approx 2\%$) to the right of plane strain. This displacement is similar to that often found in FLDs of virgin materials and may result from the combination of two effects. One is the fact that, in stretching over a dome, the strains measured on the outside surface are greater than those at the mid-plane by $\Delta\varepsilon_1 = \Delta\varepsilon_2 = t/D \approx 1\%$. The other factor is that, during the subsequent loading, the very first strain is in biaxial tension as the sheet conforms to the punch. If the sheet does not slip on the punch the level of this causes a biaxial strain at the mid-plane of about $\Delta\varepsilon_1 = \Delta\varepsilon_2 \approx 1\%$. In the FLDs after biaxial prestraining [Fig. 3b], the minima followed a line of constant effective strain and are displaced downward and to the right by the amount of the biaxial prestrain ($\Delta\varepsilon_1 = -1\%$ and $\Delta\varepsilon_2 = +1\%$). The net

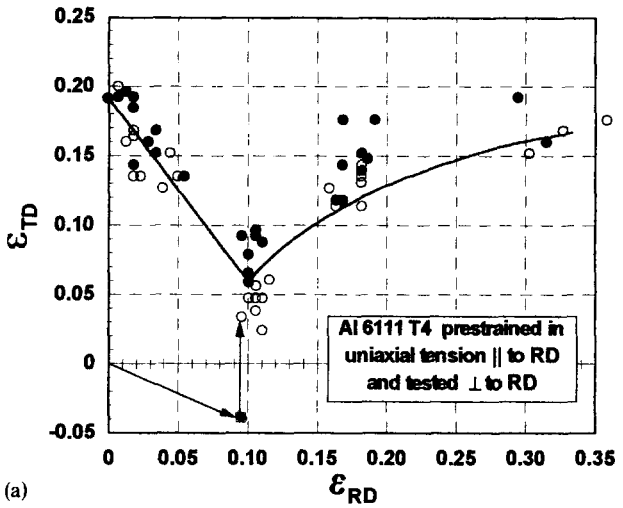


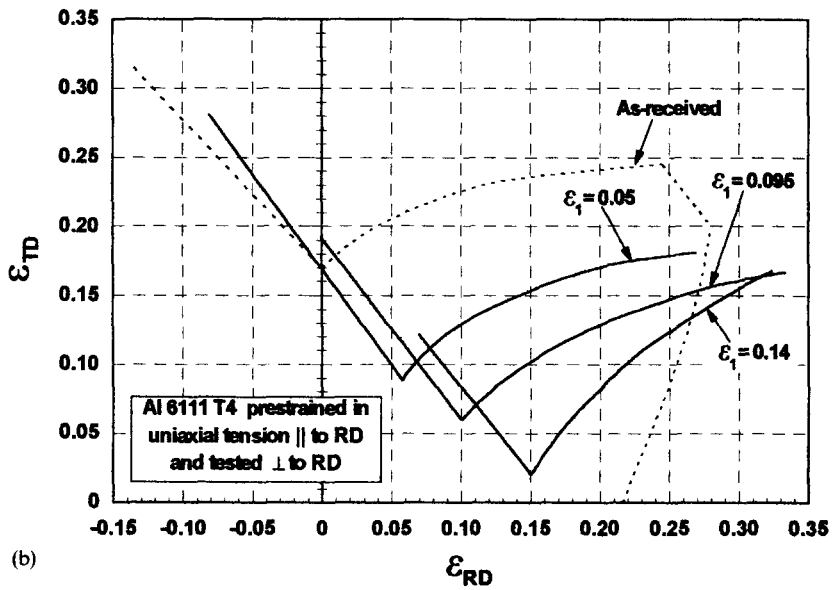


FIG. 6. (a) FLD for $\varepsilon_1$ normal to RD after uniaxial prestrain $\varepsilon_1 = 0.095$ parallel to RD; and (b) FLDs for as-received and prestrained specimens. Note that FLDo follows approximately a constant thinning line. Note the steeper slope of the RHS of the FLD after $\varepsilon_1 = 0.14$ relative to the overall trend; (c) FLDs from (b) plotted with the major and minor principal strains during prestrain added to those in final straining, regardless of their directions in the material; and (d) FLD for $\varepsilon_1$ normal to RD after uniaxial prestrain $\varepsilon_1 = 0.14$ parallel to RD.

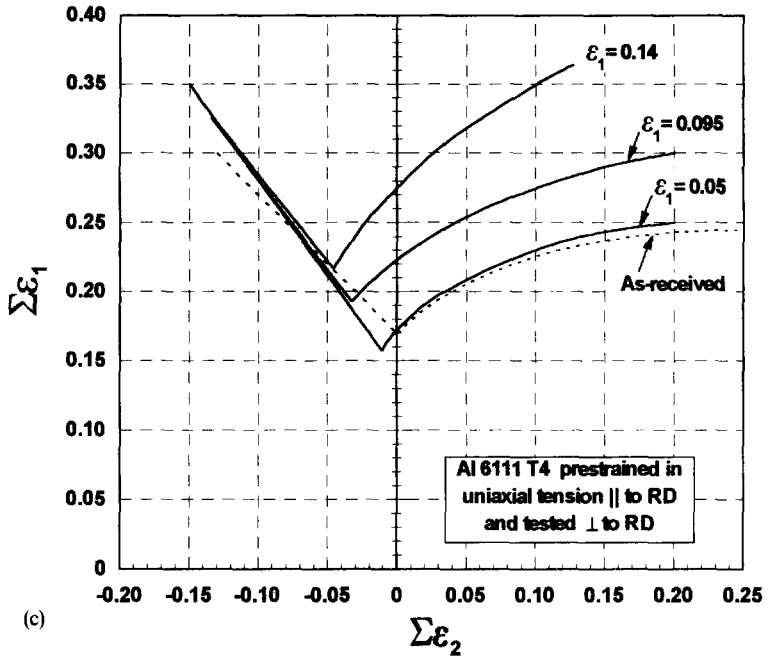


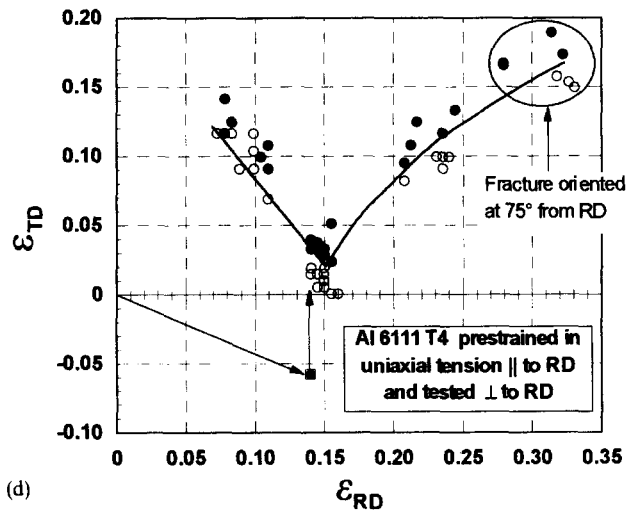


FIG. 6. (*continued*).

sum of these two effects would be to shift the minima about $\Delta\varepsilon_2 \approx 2\%$ to the right with no shift in $\varepsilon_1$. The increase of the strain limits in uniaxial tension for the prestrained specimens is consistent with the recovery reported in Fig. 4(a).

Figure 6(a) is an example of an FLD for case (2) and Fig. 6(b) summarizes the FLDs for three levels of uniaxial prestrain. The positions of the minima in Fig. 6(b) follow a constant thinning trend as for case (1), although in the opposite direction. The same data are plotted in Fig. 6(c) with the major and minor strains for prestrain, respectively, added to those for final straining regardless of their direction in the material. Replotted this way, a similarity to Fig. 5(b) is apparent.

Another interesting observation for case (2) was a shift in the fracture orientation for equibiaxially stretched specimens that have been heavily prestrained ($\varepsilon_1 = 0.14$). In these specimens, the neck formed at approximately 75° to the RD instead of being parallel to it as observed in all the other tests. This neck angle may be controlled by defects generated

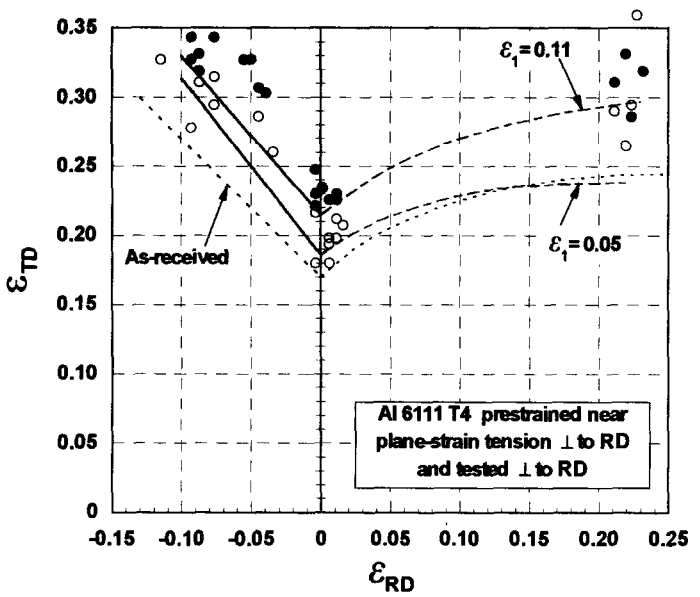


FIG. 7. FLDs obtained for $\varepsilon_1$ normal to RD after prestraining near plane strain normal to RD. Note the increase of the level of the minima with prestrain. Data are shown only for the FLD after prestrain $\varepsilon_1 = 0.11$.

during the tensile prestrain, but is larger than the angle predicted by the Hill analysis [10] $\tan\theta = \sqrt{(R+1)/R} \approx 58°$, which would increase to about 60° during the biaxial stretching. Related to this shift is the slope of the RHS of the FLD for $\varepsilon_1 = 0.14$, which is steeper than for lower levels of prestrain.

*FLDs of sheets prestrained near plane strain*

Two sets of samples were prestrained in plane strain. In one set, $\varepsilon_1$ was normal to the RD and in the other, $\varepsilon_1$ was parallel to the RD. Both sets were then tested with $\varepsilon_1$ normal to the RD.

Figure 7 shows the FLDs for two levels of prestrain near plane strain normal to the RD [case (1)] along with the as-received FLD. As previously found for Al 2008 T4 [8], no successful tests could be made for strain states between biaxial tension and plane strain, so the dashed trend lines drawn in Fig. 7 are estimations. The curve for the 5% prestrain is nearly the same as that for the as received material, the limits in biaxial tension being almost identical. The increase of the minima for the prestrained sheets is similar to those for biaxial and uniaxial tension, as in all three cases the prestrain and final paths are the same. Again, recovery during the time between pre- and final straining is probably responsible.

Figure 8(a) shows the outlines of FLDs for $\varepsilon_1$ normal to RD after prestraining in plane strain tension parallel to RD [case (2)]. As in Fig. 6(c), the FLDs in Fig. 8(b) are drawn with the major and minor principal strains during prestrain added to those during subsequent testing, regardless of the orientation of the deformation. It can be seen that for the lower prestrain, the level of the minimum is unchanged but it increases for the higher prestrain. The forming limits near equibiaxial tension are higher than those in Fig. 7. The reason is that, during prestraining parallel to RD, ridging does not develop, so the localization of necking does not start until the final deformation. In contrast, for the FLDs in Fig. 7, ridging develops during prestraining and accelerates the formation of localized necks.

## FORMING LIMITS IN PLANE STRAIN AFTER VARIOUS PRESTRAIN PATHS

The level of the FLD minimum is of particular interest, since most of the failures in sheet metal forming occur at, or near, plane strain. For complex strain-paths, the location and level of the minima depend on the deformation during prestrain. However, a simple trend

emerges when amount of additional plane strain achievable after prestrain is plotted as a function of the prestrain expressed as effective strain (Fig. 9). For simplicity, the effective strains, $\bar{\varepsilon}$, were calculated assuming planar isotropy,† from the following yield criterion suggested for fcc metals [11],

$$(\bar{R} + 1)\bar{\sigma}^8 = \sigma_1^8 + \sigma_2^8 + \bar{R}(\sigma_1 - \sigma_2)^8, \tag{1}$$

and from the flow rules

$$\rho = \frac{d\varepsilon_2}{d\varepsilon_1} = \frac{\alpha_1 - \bar{R}(1-\alpha)^7}{1 + \bar{R}(1-\alpha)^7}, \tag{2}$$

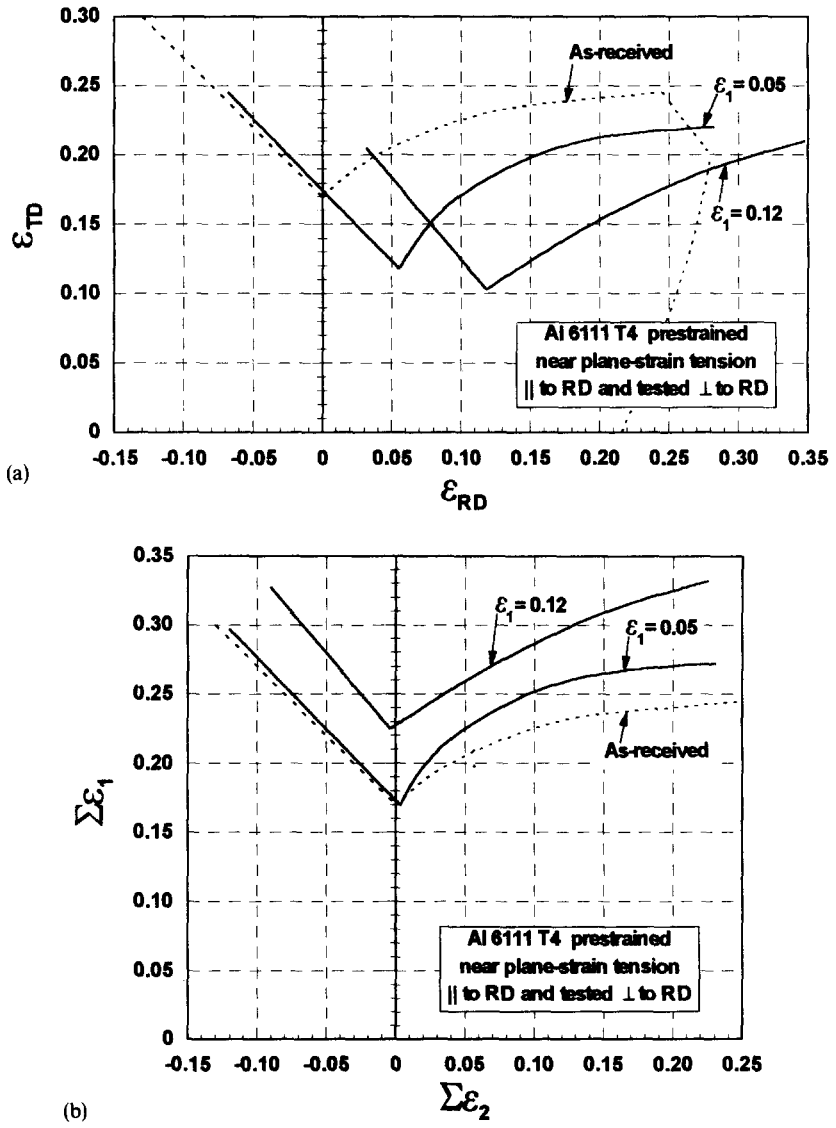


FIG. 8. (a) FLDs for the as-received and prestrained specimens. The minimum for the highest prestrain does not follow the constant thinning trend; and (b) FLDs from (a) plotted with the major strains during prestrain added to the major strains during final straining.

† Effective strains calculated taking into account planar anisotropy are almost identical because of the high exponent in the yield criterion which minimizes the $R$ value differences between sheet orientations.

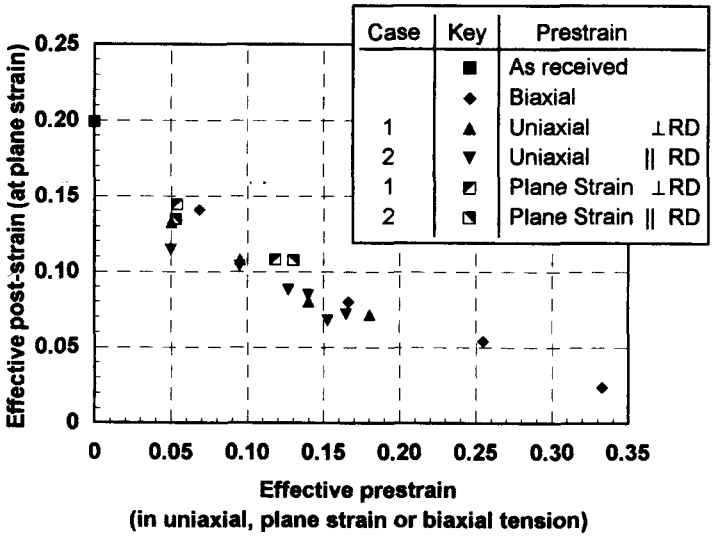


FIG. 9. Effective post-strain at plane strain ($\varepsilon_2 = 0$) as a function of initial effective prestrain. Effective strains were calculated using Eqns (1–4). All post-strains are normal to the RD.

where $\alpha = \sigma_2/\sigma_1$. From the definition of incremental plastic work for plane stress loading:

$$dw = \bar{\sigma}d\bar{\varepsilon} = \sigma_1 d\varepsilon_1 + \sigma_2 d\varepsilon_2 = \sigma_1 d\varepsilon_1(1 + \alpha\rho) \tag{3}$$

and

$$d\bar{\varepsilon} = d\varepsilon_1 \zeta(1 + \alpha\rho) \quad \text{with} \quad \zeta = \sigma_1/\bar{\sigma}, \quad \rho = \varepsilon_2/\varepsilon_1 \quad \text{and} \quad \alpha = \sigma_2/\sigma_1. \tag{4}$$

The value of $\alpha$ must be obtained numerically from Eqn (2). Assuming linear strain paths for pre- and post-strains, the differential operators are not necessary in these equations. For small prestrains, the obtainable deformation in plane strain after prestraining decreases almost linearly, following a line of constant effective strain, but it deviates from linearity and asymptotically approaches zero for higher prestrains. Such positive deviations from a constant effective strain line have been explained by the transient effects in the initial deformation after reloading [8].

## INDUSTRIAL OBSERVATIONS

Because of strain-path changes during the stamping of parts, there are instances in which the FLD for the as-received material cannot account for the observed failures. Many of these occur when features such as *embossments*, character lines or reinforcement ribs are imposed over an almost fully conformed part at the end of the punch travel. The levels of the strains required to form such features are more important for aluminum than for steel because of the overall lower formability of the former.

Figure 10(a) is a partial view of an aluminum door frame. Plane strain with $\varepsilon_1$ normal to the binder line (the binder line, not shown, runs left to right parallel to $\varepsilon_1$ at the failure) was prevalent during most of the punch travel. Near the end, a feature to accommodate a matching part is formed imposing near plane strain with the major strain axis rotated 90° from the previous orientation. The material split at that location, even though the final strain level is below the FLD for the as-received material. Figure 10(b) shows the approximate strain-path for the site of the split. The shifting of the FLD for prestrained material explains the occurrence of the split below the FLD for the as-received material.

## CONCLUSIONS

Abrupt changes in strain-path during forming can produce significant changes in the forming limits.

- Prestrain in biaxial tension decreases the formability if followed by plane strain or biaxial tension, but there are higher forming limits in subsequent tension.

- Prestraining in uniaxial tension raised the forming limits for subsequent plane strain and biaxial tension, when the direction of the principal strains is preserved [case (1)] but decreases them if the direction when the principal strains are rotated after prestraining [case (2)].
- Prestraining in plane strain produces a slight increase of the overall level of the curve for case (1) but decreases it substantially for case (2).

The ridging developed during deformation has a detrimental effect on the strain limits normal to the orientation of the ridges.

After prestraining, the minimum of the FLD occurs at or near plane strain for subsequent FLD determination regardless of the strain-path followed during prestraining and the slight displacement to the right, observed in some FLDs, may be caused by bending strains introduced when the specimen conforms to the punch.

The level of plane strain achievable after different strain-paths followed during the prestrain all fall approximately on a single line when plotted vs the effective strain during prestrain.

The evidence, *though limited*, suggests that recovery occurs in the time between pre- and final straining, raising the forming limits.

*Acknowledgments*—The authors want to thank ALCOA Technical Center for the financial support for this investigation. We also acknowledge Ford Motor Co. Advanced Technology and Materials Engineering and National Steel Product Application Center for the use of their formability testing machines.

## REFERENCES

1. S. P. KEELER, Determination of forming limits in automotive stampings. *Sh. Metal Ind.*, 683 (1965).
2. W. MÜSCHENBORN and H. M. SÖNNE, Influence of the strain path on the forming limits of sheet metal. *Arch. Eisenhütt.* **46**, 597 (1975).
3. J. V. LAUKONIS and A. K. GHOSH, Anisotropic strain localization in tensile prestrained sheet steel. *Met. Trans.* **9A**, 1849 (1978).
4. A. J. RANTA-ESCOLA, Effect of loading path on stress–strain relationships of steel sheet and brass. *Mater. Technol.* **45**, (1980).
5. J. H. SCHMITT, J. RAPHAEL, E. RAUCH and P. MARTIN, Plastic instability of prestrained material, *Computational Methods for Predicting Materials Processing Defects*, p. 309. Elsevier, Amsterdam (1987).
6. H. SANG and D. J. LLOYD, The influence of strain path on subsequent mechanical properties. Orthogonal tensile paths. *Met. Trans.* **10A**, 1767 (1979).
7. M. ZANDRAHIMI and D. V. WILSON, Effect of changes in strain path on work hardening in cubic metals. *Met. Trans.* **20A**, 2471 (1989).
8. A. GRAF and W. F. HOSFORD, Effect of changing strain paths on forming limit diagrams of Al 2008-T4, *Met. Trans.* **24A**, 2503 (1993).
9. N. TAKAKURA, K. YAMAGUCHI and M. FUKUDA, Improvement of the forming limit of sheet metals by removal of surface roughening with plastic strain. *JSME Int. J.* **30**, 2034 (1987).
10. R. HILL, *The Mathematical Theory of Plasticity*, p. 322. Oxford University Press, London (1950).
11. W. F. HOSFORD, On yield loci of anisotropic cubic metals. *Proc. 7th N. Am. Metalworking Conf.*, p. 191, SME, Dearborn, MI (1979).